Four-Dimensional Variational Data Assimilation for WRF: Formulation and Preliminary Results

XIANG-YU HUANG, QINGNONG XIAO, DALE M. BARKER, XIN ZHANG, JOHN MICHALAKES, WEI HUANG, TOM HENDERSON, JOHN BRAY, YONGSHENG CHEN, ZAIZHONG MA, JIMY DUDHIA, YONGRUN GUO, XIAOYAN ZHANG, DUK-JIN WON, HUI-CHUAN LIN, AND YING-HWA KUO

National Center for Atmospheric Research, Boulder, Colorado*

(Manuscript received 28 February 2008, in final form 19 September 2008)

ABSTRACT

The Weather Research and Forecasting (WRF) model–based variational data assimilation system (WRF-Var) has been extended from three- to four-dimensional variational data assimilation (WRF 4D-Var) to meet the increasing demand for improving initial model states in multiscale numerical simulations and forecasts. The initial goals of this development include operational applications and support to the research community. The formulation of WRF 4D-Var is described in this paper. WRF 4D-Var uses the WRF model as a constraint to impose a dynamic balance on the assimilation. It is shown to implicitly evolve the background error covariance and to produce the flow-dependent nature of the analysis increments. Preliminary results from real-data 4D-Var experiments in a quasi-operational setting are presented and the potential of WRF 4D-Var in research and operational applications are demonstrated. A wider distribution of the system to the research community will further develop its capabilities and to encourage testing under different weather conditions and model configurations.

1. Introduction

The four-dimensional variational data assimilation (4D-Var) technique (Le Dimet and Talagrand 1986; Lewis and Derber 1985) has been pursued actively by the research community and operational centers over the past two decades. Several 4D-Var research systems have been developed, including 1) one based on the fifth-generation Pennsylvania State University–National Center for Atmospheric Research (PSU–NCAR) Mesoscale Model (MM5; Zou et al. 1995, 1997; Ruggiero et al. 2006), 2) one based on the National Centers for Environmental Prediction (NCEP) Eta Model (Zupanski 1993), 3) the 4D-Var-based Regional Atmospheric Modeling System (RAMS) data assimilation system (RAMDAS; Zupanski et al. 2005), and 4) the variational Doppler Radar assimilation system (VDRAS) for convective-scale assimilation of radar data (Sun and Crook 1997).

The first successful operational 4D-Var system was implemented at the European Centre for Medium-Range Weather Forecasts (ECMWF) using an incremental formulation (Courtier et al. 1994; Rabier et al. 1997). The results demonstrate a significant positive impact on operational forecasts compared to its 3D-Var system (Rabier et al. 2000). Following ECMWF, several operational centers implemented 4D-Var in their operational applications, including Météo-France (Gauthier and Thépaut 2001), the Met Office (Lorenc and Rawlins 2005; Rawlins et al. 2007), the Japan Meteorological Agency (Honda et al. 2005), and Environment Canada (Gauthier et al. 2007). Other operational centers are also preparing 4D-Var as their data assimilation package, including the High-Resolution Limited-Area Model (HIRLAM; Huang et al. 2002) and the Naval Research Laboratory Atmospheric Variational Data Assimilation System (NAVDAS-AR; Xu et al. 2005).

The 4D-Var technique has a number of advantages over 3D-Var schemes including:

1) The ability to use observations at the time of their measurement or in predetermined time bins (see the discussion in the next section) which suits most asynoptic data.

* The National Center for Atmospheric Research is sponsored by the National Science Foundation.

Corresponding author address: Dr. Xiang-Yu Huang, NCAR/MMM, P.O. Box 3000, Boulder, CO 80307.
E-mail: huangx@ucar.edu

DOI: 10.1175/2008MWR2577.1

2) Implicit defination of flow-dependent forecast error covariances, of vital importance in the optimal use of observations in fast-developing weather systems.
3) The ability to use a forecast model as a constraint enhancing the dynamic balance of the final analysis.

Given these advantages of 4D-Var and its demonstrated effectiveness in worldwide operations, the inclusion of 4D-Var capability within the Weather Research and Forecasting (WRF) model (Skamarock et al. 2005) should lead to improved WRF model initialization.

This paper documents the formulation and preliminary results of the 4D-Var capability developed as an extension to the current 3D-Var data assimilation system (Barker et al. 2004a,b). The 4D-Var component of the expanded 3/4D-Var system (known as WRF-Var, hereafter referred to as WRF 4D-Var; Barker et al. 2005) has undergone extensive development since 2004. The initial prototype (completed in 2005) has been continuously refined. It uses the Advanced Research WRF (ARW; Skamarock et al. 2005) dynamical core and 3D-Var as its basic components (Huang et al. 2005). The WRF tangent linear and adjoint models are based on a simplified WRF model. They have been successfully applied in adjoint sensitivity studies of an Antarctic severe windstorm (Xiao et al. 2008). Initial standard assimilation (i.e., linear, adjoint, and single observation) tests have been carried out to validate the 4D-Var formulation. A series of real-data experiments have also been conducted to assess the performance of 4D-Var (Huang et al. 2006).

The rest of this paper is laid out as follows. In section 2, the incremental 4D-Var approach used for WRF 4D-Var is summarized. Section 3 presents results from standard single observation test experiments to illustrate the flow-dependent nature of 4D-Var analysis increments. Preliminary results from real-data experiments are presented in section 4. Finally, conclusions and plans for future work are described in section 5.

2. The WRF 4D-Var algorithm

The WRF 4D-Var algorithm takes the incremental 4D-Var formulation that is commonly used in operational systems (Courtier et al. 1994; Veersé and Thépaut 1998; Lorenc 2003). The incremental approach is designed to find the analysis increment that minimizes a cost function defined as a function of the analysis increment instead of the analysis itself. In the incremental 4D-Var, the tangent linear and adjoint models usually derived from a simplified forward model are used in the inner-loop minimization, while the evolution of the background is predicted with the full forward model. The current WRF 4D-Var system makes use of the following components of the previously developed WRF-Var system (Barker et al. 2005): 1) observation operators, 2) quality control, 3) the background error covariance model, 4) a minimization inner-loop using simplified WRF tangent linear and adjoint models and assuming Gaussian error covariances, and 5) an iterative outer loop using the nonlinear WRF model to update the basic trajectory state to account for the effect of nonlinearities in the assimilation algorithm.

Mathematically WRF 4D-Var minimizes a cost function J:

$$J = J_b + J_o + J_c, \tag{1}$$

which includes quadratic measure of distance to the background, observation, and balanced solution. The background cost function term J_b is

$$\begin{aligned} J_b &= \frac{1}{2}(\mathbf{x}^n - \mathbf{x}^b)^{\mathrm{T}}\mathbf{B}^{-1}(\mathbf{x}^n - \mathbf{x}^b) \\ &= \frac{1}{2}[(\mathbf{x}^n - \mathbf{x}^{n-1}) + (\mathbf{x}^{n-1} - \mathbf{x}^b)]^{\mathrm{T}}\mathbf{B}^{-1}[(\mathbf{x}^n - \mathbf{x}^{n-1}) \\ &\quad + (\mathbf{x}^{n-1} - \mathbf{x}^b)] \\ &= \frac{1}{2}\left[(\mathbf{x}^n - \mathbf{x}^{n-1}) + \sum_{i=1}^{n-1}(\mathbf{x}^i - \mathbf{x}^{i-1})\right]^{\mathrm{T}}\mathbf{B}^{-1}\left[(\mathbf{x}^n \right. \\ &\quad \left. - \mathbf{x}^{n-1}) + \sum_{i=1}^{n-1}(\mathbf{x}^i - \mathbf{x}^{i-1})\right], \end{aligned} \tag{2}$$

where superscripts -1 and T denote inverse and adjoint of a matrix or a linear operator. Here $\mathbf{B}$ is the background error covariance matrix, which is typically climatological estimates, but it may also be derived from prior or ensemble-based flow-dependent estimates or, with slightly different formulation, combination of both climatological and ensemble estimates (e.g., Buehner 2005). In this study, the climatological estimate of $\mathbf{B}$ is used. The background $\mathbf{x}^b$ is usually a short-range forecast from a previous analysis. In a slight abuse of notation, the analysis vector $\mathbf{x}^i$ denotes an intermittent analysis after the ith outer loop. The outer loop index i varies from 1 to n, where n is the desired total number of outer loop. The final analysis of WRF 4D-Var after the last (nth) outer loop is denoted as $\mathbf{x}^n$ or equivalently $\mathbf{x}^a$.

The inner-loop minimization starts from a guess vector, $\mathbf{x}^{n-1}$ (the analysis vector from the last second outer loop). For the first outer loop, $\mathbf{x}^b$ is normally taken as the guess vector, $\mathbf{x}^0$. It should be stressed that the background vector and the guess vector should not be mixed in the incremental formulation. They are the same only during the first outer loop.

The observation cost function term represents the quadratic measure of distance between the analysis $\mathbf{x}^n$, through the forecast model M_k and the observation operator H_k, and the observations $\mathbf{y}_k$:

$$\begin{aligned} J_o &= \frac{1}{2}\sum_{k=1}^{K}\{H_k[M_k(\mathbf{x}^n)] - \mathbf{y}_k\}^{\mathrm{T}}\mathbf{R}^{-1}\{H_k[M_k(\mathbf{x}^n)] - \mathbf{y}_k\} \\ &\approx \frac{1}{2}\sum_{k=1}^{K}\{H_k[M_k(\mathbf{x}^{n-1})] + \mathbf{H}_k\mathbf{M}_k(\mathbf{x}^n - \mathbf{x}^{n-1}) - \mathbf{y}_k\}^{\mathrm{T}} \\ &\quad \times \mathbf{R}^{-1}\{H_k[M_k(\mathbf{x}^{n-1})] + \mathbf{H}_k\mathbf{M}_k(\mathbf{x}^n - \mathbf{x}^{n-1}) - \mathbf{y}_k\} \\ &= \frac{1}{2}\sum_{k=1}^{K}[\mathbf{H}_k\mathbf{M}_k(\mathbf{x}^n - \mathbf{x}^{n-1}) - \mathbf{d}_k]^{\mathrm{T}}\mathbf{R}^{-1} \\ &\quad \times [\mathbf{H}_k\mathbf{M}_k(\mathbf{x}^n - \mathbf{x}^{n-1}) - \mathbf{d}_k]. \end{aligned} \tag{3}$$

Here a linear approximation is made. The whole assimilation time window is split into K observation windows. Here H_k and $\mathbf{H}_k$ are the nonlinear and tangent linear observation operators, respectively, over observation window k ($k = 1, K$) transforming atmospheric variables from the gridded analysis space to the observation space. Here M_k and $\mathbf{M}_k$ are the nonlinear and tangent linear models, respectively, propagating the guess vector $\mathbf{x}^{n-1}$ and analysis increments $\mathbf{x}^n - \mathbf{x}^{n-1}$ from the first to the kth observation time window. Here $\mathbf{d}_k$ is the innovation vector for observation window k:

$$\mathbf{d}_k = \mathbf{y}_k - H_k[M_k(\mathbf{x}^{n-1})]. \tag{4}$$

Finally, $\mathbf{R}$ is the observation error covariance matrix.

The balancing cost function term measures the quadratic distance between the analysis and a balanced state. As an initial application, a digital filter is included in WRF 4D-Var to remove the high-frequency waves in the analysis. The digital filter in J_c formulation implemented in WRF 4D-Var is similar to the forms in Gustafsson (1992), Gauthier and Thépaut (2001), and Wee and Kuo (2004):

$$\begin{aligned} J_c &= \frac{1}{2}\gamma_{df}[\mathbf{M}_{N/2}(\mathbf{x}^n - \mathbf{x}^{n-1}) \\ &\quad - \sum_{i=0}^{N} f_i\mathbf{M}_i(\mathbf{x}^n - \mathbf{x}^{n-1})]^{\mathrm{T}}\mathbf{C}^{-1}[\mathbf{M}_{N/2}(\mathbf{x}^n - \mathbf{x}^{n-1}) \\ &\quad - \sum_{i=0}^{N} f_i\mathbf{M}_i(\mathbf{x}^n - \mathbf{x}^{n-1})] \\ &= \frac{1}{2}\gamma_{df}\left[\sum_{i=0}^{N} g_i\mathbf{M}_i(\mathbf{x}^n - \mathbf{x}^{n-1})\right]^{\mathrm{T}}\mathbf{C}^{-1} \\ &\quad \times \left[\sum_{i=0}^{N} g_i\mathbf{M}_i(\mathbf{x}^n - \mathbf{x}^{n-1})\right], \end{aligned} \tag{5}$$

where f_i is the coefficient for the digital filter (Lynch and Huang 1992; Gauthier and Thépaut 2001); g_i is the modified coefficient, where $g_i = -f_i$ for i $\neq N/2$ and $g_{N/2} = 1 - f_{N/2}$. Also, N is the total integration steps over the assimilation window, γ_{df} is the weight assigned to J_c term, and $\mathbf{C}$ is a diagonal matrix containing variances of wind, temperature, and dry surface pressure with values of $(3\ \mathrm{m\ s^{-1}})^2$, $(1\ \mathrm{K})^2$, and $(10\ \mathrm{hPa})^2$, respectively.

To reduce the condition number and to accelerate the minimization algorithm, the preconditioning of the background cost function is implemented by a control variable transform:

$$\mathbf{v}^n = \mathbf{U}^{-1}(\mathbf{x}^n - \mathbf{x}^{n-1}), \tag{6}$$

where $\mathbf{U}$ is defined as $\mathbf{B} = \mathbf{U}\mathbf{U}^{\mathrm{T}}$ (Barker et al. 2005). The cost function gradient J' with respect to the control variable $\mathbf{v}^n$ is

$$\begin{aligned} J'(\mathbf{v}^n) &= \sum_{i=1}^{n-1}\mathbf{v}^i + \mathbf{v}^n \\ &\quad + \mathbf{U}^{\mathrm{T}}\sum_{k=1}^{K}\mathbf{M}_k^{\mathrm{T}}\mathbf{H}_k^{\mathrm{T}}\mathbf{R}^{-1}\{\mathbf{H}_k\mathbf{M}_k\mathbf{U}\mathbf{v}^n - \mathbf{d}_k\} \\ &\quad + \mathbf{U}^{\mathrm{T}}\sum_{i=0}^{N}\mathbf{M}_i^{\mathrm{T}}f_i\gamma_{df}\mathbf{C}^{-1}\left(\sum_{i=0}^{N} f_i\mathbf{M}_i\mathbf{U}\mathbf{v}^n\right). \end{aligned} \tag{7}$$

Here $\mathbf{H}_k^{\mathrm{T}}$ is the adjoint observation operator over observation window k; $\mathbf{M}_k^{\mathrm{T}}$ is the adjoint model, which propagates the analysis residuals, {.} in Eq. (7), and the digital filter forcing, (.) in Eq. (7), backward in time from the time as indicated by the indices, i or k, to 0. Note that a 3D-Var solution can be obtained by setting $K = 1$ and removing model-related components. The detailed descriptions of the WRF 4D-Var data flow and program structure can be found in the appendix.

Figure 1 shows a typical example of the cost functions (J_o, J_b, and J_c) and the gradient norm evolving as functions of minimization simulations (iterations). The case is Typhoon Haitang (2005) at 0000 UTC 16 July 2005, and the 4DVAR experiment includes all conventional observations (see section 4 for details). For this particular case, WRF 4D-Var reaches the minimum, defined as the gradient norm reduces to 1% of its original value, in 22 iterations. After the minimization converges, the cost function reduces to about half of its original value. The experiments for other cases, such as severe convective storms and hurricanes in the Atlantic Ocean, typically show convergence in less than 100 iterations.

To give readers an idea about the computational cost, the detailed running time on NCAR's IBM supercomputer *blueice* is listed here. The 22-iteration

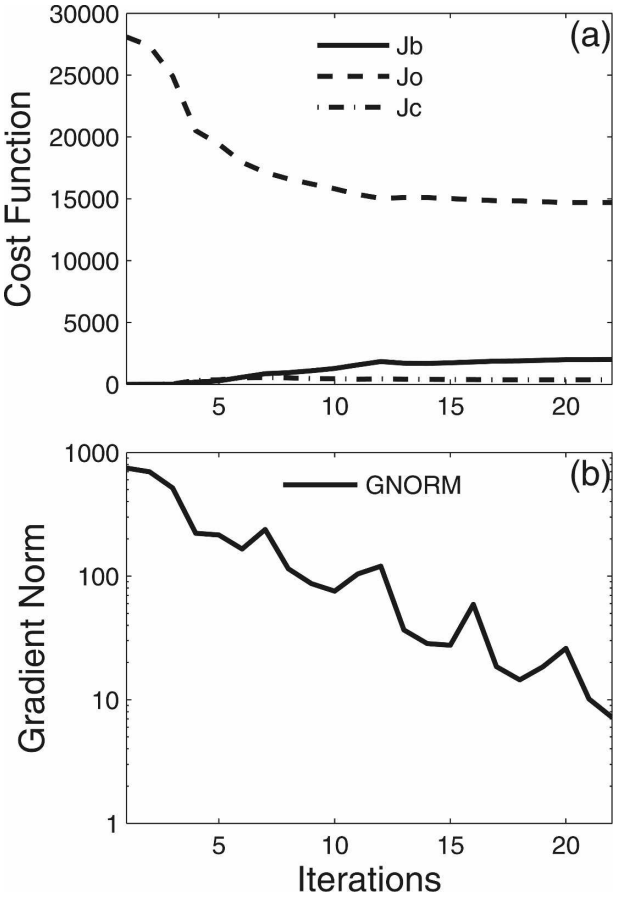

FIG. 1. The (a) cost functions (J_b, J_o, and J_c) and (b) gradient norm as functions of minimization simulations (iterations).

4D-Var analysis takes about 1.5-h wall clock time and 5-GB memory on 64 power5+ processors. Within one iteration, the nonlinear, adjoint and tangent linear models take about 35, 105, and 37 s, respectively. Note that there are 1–2 disk I/O (reading or writing netcdf files) in every time step for each model. Future development will eliminate disk I/O to further reduce the running time.

3. WRF 4D-Var structure functions

Analysis increments due to a single observation produced by a data assimilation system implicitly provide the effective background error covariance matrix **B**, often referred to as structure functions (Thépaut et al. 1996). The idea behind the single observation test in 3D-Var is that the analysis increment $\boldsymbol{x}^a - \boldsymbol{x}^b$ is proportional to the background error covariance by assuming an observation of a single model variable:

$$\boldsymbol{x}^a - \boldsymbol{x}^b = \mathbf{B}_i(\sigma_b^2 + \sigma_o^2)^{-1}(y_i - x_i), \quad (8)$$

where y_i is the single observation at the ith grid point, x_i is its corresponding equivalence calculated from the background, and σ_o and σ_b are the observation and background errors, respectively. Here **B** is the background error covariance and $\mathbf{B}_i$ is the ith column. In WRF 4D-Var, the tangent linear model **M** and its adjoint $\mathbf{M}^{\mathrm{T}}$ are directly involved in the analysis procedure. The 4D-Var solution for assimilation of the single observation y_i becomes

$$\mathbf{M}(x^a - x^b) = (\mathbf{MBM}^{\mathrm{T}})_i(\sigma_b^2 + \sigma_o^2)^{-1}(y_i - x_i). \quad (9)$$

The spread of information around the single observation depends on not only the background error covariance matrix, but also the tangent linear and adjoint model integration. In other words, the model plays a role in propagating the observed information in the 4D-Var analysis. A single observation test can clearly show that structure.

After the WRF 4D-Var system was developed, we carried out many single observation experiments to compare the implicit structure functions of WRF-Var in 3D-Var and 4D-Var modes. An example of these experiments shown in this section is a severe winter storm case that occurred at 0000 UTC 25 January 2000 (Zupanski et al. 2002; Jang et al. 2003). We used a 6-h forecast valid at 0000 UTC 25 January 2000 as the background for both 3D-Var and 4D-Var. A single temperature observation at 0600 UTC is placed at 30°N, 75°W, 500 hPa. This case is deliberately constructed with an overly large 6-h observation/analysis time difference to demonstrate one of the potential problems related to 3D-Var when assimilating asynoptic observations. Typically the time differences are 3 h or less when the first guess at appropriate time (FGAT) 3D-Var technique is used.

The 3D-Var increments (Fig. 2a) show an isotropic structure centered at the observation location. As suggested by Eq. (8), this is a graphic presentation of the background error covariance matrix, **B**, or 3D-Var structure function. The increments are added to the background at the analysis time to produce the 3D-Var analysis. Two forecasts using WRF are then made: one initialized from the background and the other from the analysis. The differences between the two forecasts are shown in Fig. 2. In this particular case, when the observation and analysis times are 6 h apart the changes made by the 3D-Var assimilation of observation produce little impact on the model fields at the time and location of the observation.

The 4D-Var increments have a temporal dimension as shown in Fig. 3. The increments at 6 h (Fig. 3g) give a graphic representation of the background error co-

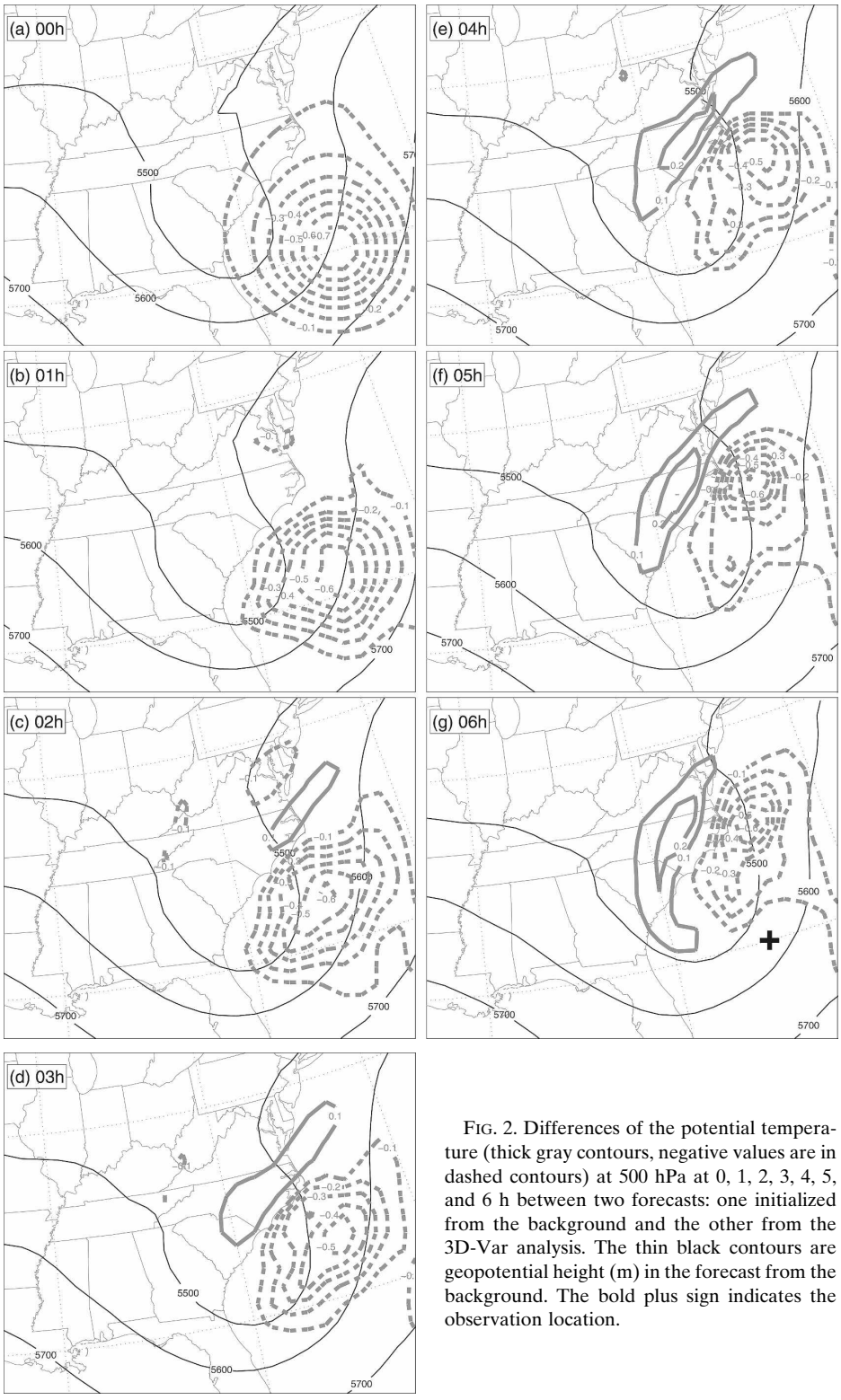

FIG. 2. Differences of the potential temperature (thick gray contours, negative values are in dashed contours) at 500 hPa at 0, 1, 2, 3, 4, 5, and 6 h between two forecasts: one initialized from the background and the other from the 3D-Var analysis. The thin black contours are geopotential height (m) in the forecast from the background. The bold plus sign indicates the observation location.

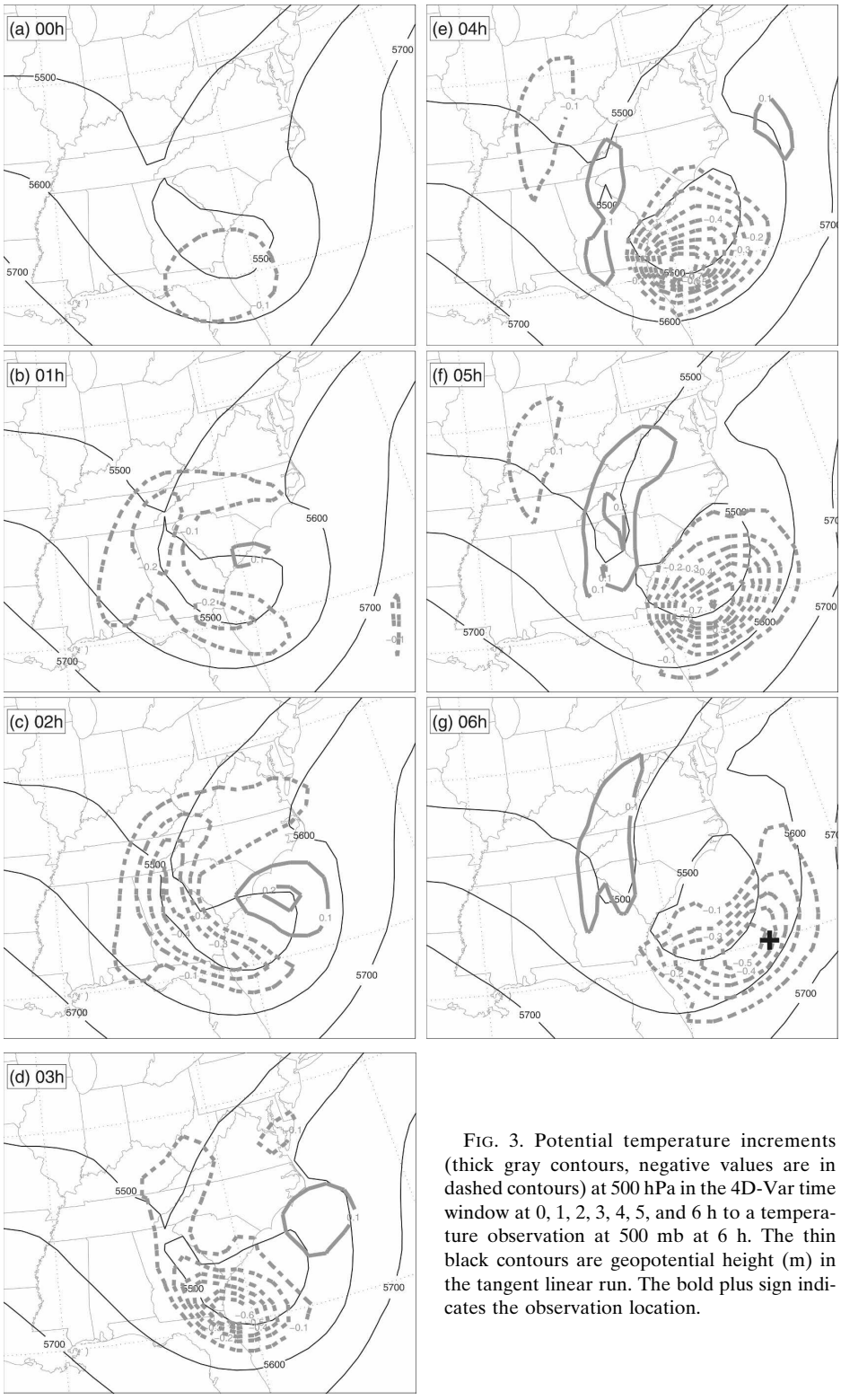

FIG. 3. Potential temperature increments (thick gray contours, negative values are in dashed contours) at 500 hPa in the 4D-Var time window at 0, 1, 2, 3, 4, 5, and 6 h to a temperature observation at 500 mb at 6 h. The thin black contours are geopotential height (m) in the tangent linear run. The bold plus sign indicates the observation location.

variance matrix at 6 h, $\mathbf{MBM}^{\mathrm{T}}$, or 4D-Var structure function. In addition to providing a fit to the observation at the observation location, it has a clear flow-dependent nature. Zhang (2005) studied the covariance structures using short-term ensemble forecast for the same case. Though different locations and different variables were chosen for the calculation, similar elongated flow-dependent covariance structure was obtained. The increments at the analysis time (0 h; Fig. 3a) are small with a center upstream of the observation. The 4D-Var analysis is obtained by adding the increments at 0 h to the background. Again, the differences between two forecasts, one initialized from the background and the other from the 4D-Var analysis are shown in Fig. 4. The 6-h forecast from the 4D-Var analysis has smaller errors relative to the observation. The fact that the potential temperature increments in Fig. 3 and the forecast differences in Fig. 4 are similar suggests that the linear approximations in 4D-Var are reasonable for this case. There is no dramatic degradation due to the approximation of linearity in the evolution of the analysis increments. The mismatch between Figs. 3 and 4 may be related to two factors. One is that the nonlinear model is different (new version) from the simplified version of the nonlinear model used to develop tangent linear and adjoint models. The other possible reason is that the weather system is nonlinear in nature (Zhang et al. 2002, 2003, 2007). The nonlinear growth of the initial error may also lead to significant differences in forecasts at 6 h.

The advantage of WRF 4D-Var analysis compared with WRF 3D-Var is its flow-dependent structure in the increments. 4D-Var implicitly evolves the background covariances in time. On the contrary, 3D-Var can only use the static covariance in the analysis, and its resulting increments correspond exactly to the structure of the background error covariance matrix $\mathbf{B}$, which is usually homogeneous and isentropic. The flow-dependent structure function in 4D-Var is important in the analysis of fast-evolving systems, such as convective storms, squall lines, hurricanes, and cyclones, in which the structural differences of the increments as shown above will be significant even when smaller time mismatches are used. In the following sections, we will show that WRF 4D-Var obtains better analyses and subsequent forecasts than WRF 3DVAR in two selected cases.

4. Real-data 4D-Var experiments

To assess the performance of 4D-Var, a series of experiments have been conducted for severe weather cases using real observations. The cases chosen here include Typhoon Haitang which hit Taiwan on 18 July 2005 (Guo et al. 2006) and a strong cyclone that caused heavy precipitation over the Korean peninsula. The 4D-Var algorithm is tested in both cold start (the first guess for WRF-Var is 6-h ARW forecast from a global analysis) and cycling (the first guess is the 6-h short-range WRF forecast initialized from the previous WRF-Var analysis) modes.

a. Cold-start assimilation

Typhoon Haitang (2005) originated from a poorly organized depression that formed west of Marcus Island on 11 July 2005. It reached tropical storm strength quickly, and became a typhoon at 1800 UTC 12 July. It intensified to a category 5 supertyphoon on 16 July, but decayed to category 3 before it hit Taiwan at 0000 UTC 18 July. It weakened to a tropical storm after it took a day to cross the island. It reorganized into a typhoon again over the South China Sea, and made landfall for the second time near Wenzhou China at 1200 UTC 19 July. Typhoon Haitang (2005) caused severe flash floods and landslides in Taiwan and massive evacuations in mainland China.

The designed cold-start experiments cover the period from the time when Haitang reached its peak intensity to the time when it dissipated over China. Five sets of forecast experiments are performed. Each set has nine 48-h forecasts initialized at nine different *analysis times* starting from 0000 UTC 16 July (denoted as 1600) to 0000 UTC 18 July (1800) with 6-h apart. Five sets of forecasts differ by their initial conditions described as following:

- FGS: The forecast initialized from interpolated NCEP Global Forecast System (GFS) analysis 6 h earlier than the analysis time. Its 6-h (3-h) forecast serves as the background field or first guess for the 3DVAR (FGAT and 4DVAR) data assimilation experiment.
- AVN: The forecast from the interpolated NCEP GFS analysis at the 3DVAR analysis time.
- 3DVAR: The forecast from the 3D-Var analysis. The 3D-Var analysis uses FGS fields as the first guess to assimilate observations collected from −3 to +3 h around the analysis time. Note that the same-type higher-than-6-h-frequency observations at the same location (e.g., hourly surface observations) will be thinned to one observation whose time is the closest to the analysis time. The background error covariance matrix is generated from 1-month-long forecasts in July 2005 using the National Meteorological Center (NMC) method (Parrish and Derber 1992). The same background error covariance matrix is used in

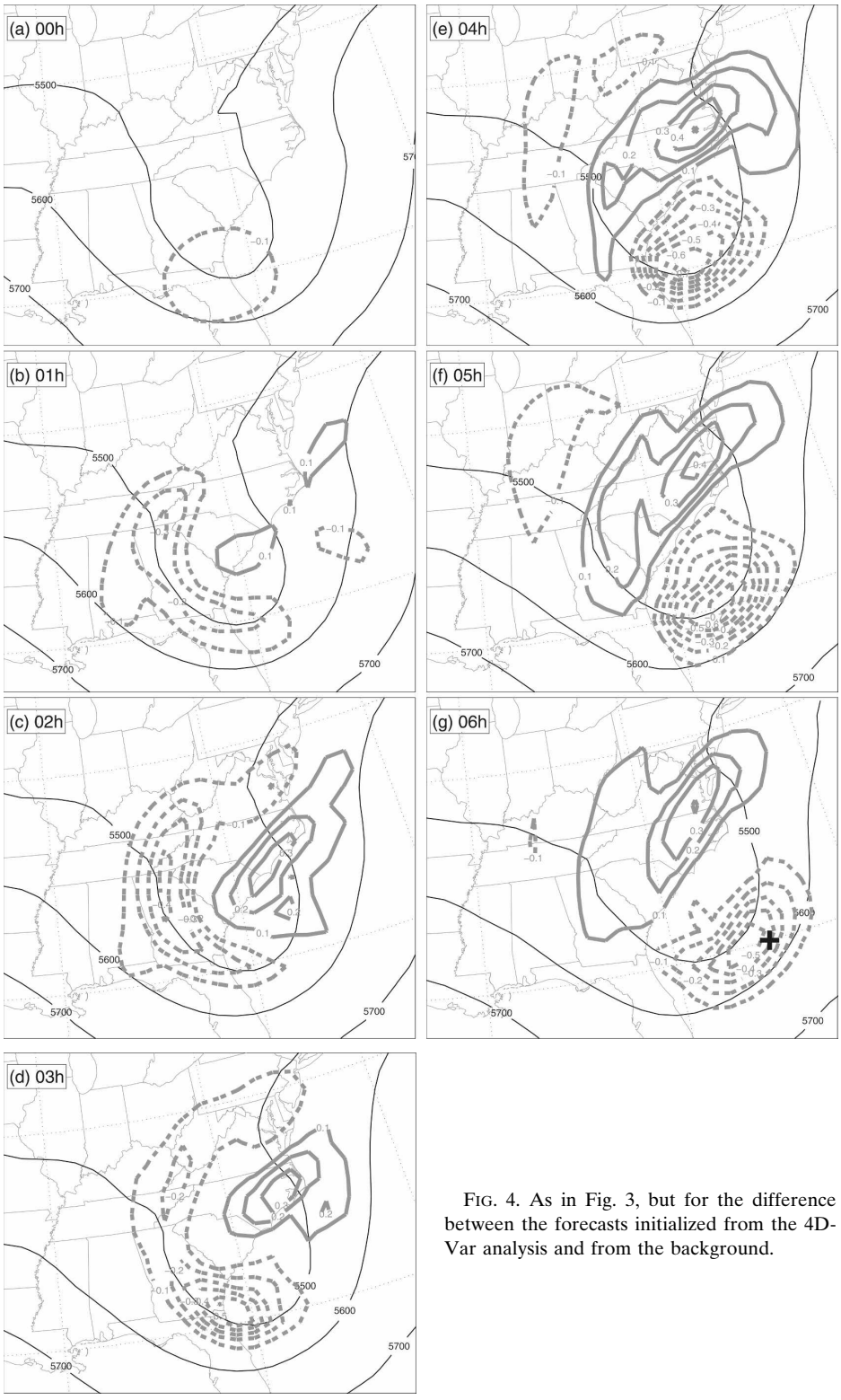

FIG. 4. As in Fig. 3, but for the difference between the forecasts initialized from the 4D-Var analysis and from the background.

TABLE 1. The number of different types of observations assimilated by 4DVAR at 0000 UTC 16 Jul 2005.

Obs type	u	v	T	p	q	DZ
TEMP	1139	1130	1435		1153	
SYNOP	668	690	644	677	637	
SATOB	2668	2668				
AIREP	528	528	532			
PILOT	139	139				
METAR	363	365	446		436	
SHIP	57	57	61	61	56	
SATEM						441
BUOY	79	77	5	66		
BOGUS	607	607	399	40	399	

FGAT and 4DVAR experiments. The lateral and lower boundary conditions along with their time tendencies generated from GFS analyses are updated using the boundary values in the 3D-Var analysis, so that the boundary values at analysis time are identical to the new analysis at the analysis time and the boundary values at future times still matches previous GFS target values.

- FGAT: This forecast is an option of 3D-Var (Lee and Barker 2005; Huang et al. 2005) analysis. In this experiment, the observations in the same time window as in 3DVAR are binned hourly. The innovations are computed using the basic states at the corresponding time bins, but then the innovations are treated as if they are valid at the same analysis time as in 3DVAR. The boundary conditions are updated in the same manner as in 3DVAR.
- 4DVAR: The forecast from the 4D-Var analysis. The 4D-Var analysis has a 6-h time window centered at the analysis time. The same hourly binned observations as in FGAT are assimilated. It uses 3-h FGS forecast as the background to produce the analysis at the beginning of the 6-h time window (i.e., −3 h). The model is then advanced 3 h to the analysis time. The model lateral and lower boundaries are updated similarly to 3DVAR experiments except done twice: one at −3 h and the other at the analysis time.

The same domain configuration and physical parameterization options are used for all forecast runs. The model domain has 91 × 73 × 17 grid points with a 45-km horizontal spacing and 4-min time steps. The ARW model used in the forecast employs the WRF Single-Moment 5-class (WSM5) microphysics scheme (Hong et al. 2004), Grell–Devenyi ensemble cumulus scheme (Grell and Devenyi 2002), and the Yonsei University (YSU) boundary layer scheme.

The assimilated observations include conventional data, satellite data, and vortex bogus data from the Central Weather Bureau of Taiwan. Table 1 lists the numbers of different types of observations in a 6-h time window, from 2100 UTC 15 July to 0300 UTC 16 July. At other analysis times, there are also GPS refractivity (N) data and Quick Scatterometer (QuikSCAT) wind (QS-u, QS-v) data (e.g., 207 N, 2587 QS-u, and 2596 QS-v at 0600 UTC 16 July).

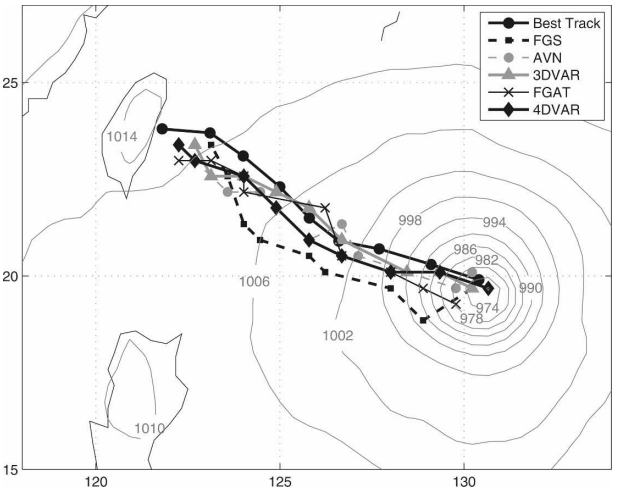

FIG. 5. The 48-h forecast typhoon tracks from FGS, AVN, 3DVAR, FGAT, and 4DVAR, together with the observed best track. Forecasts are all started from 0000 UTC 16 Jul 2005. The initial sea level pressure field (hPa) from 4DVAR is also shown in contours.

The 48-h forecasts of the typhoon track, all started at 0000 UTC 16 July 2005, are plotted in Fig. 5 together with the observed track. The sea level pressure field at initial time in 4DVAR is also shown in the figure. The forecast initialized from FGS is least successful for most lead times in this case. The forecast from AVN is improved because of updated initial conditions from the NCEP 3D-Var analysis system. Other data assimilation experiments (3DVAR, FGAT, and 4DVAR) using FGS as the background also significantly improve the track forecast. The 48-h-averaged track forecast error is reduced from 125 km in FGS to about 60 km in 3DVAR and 4DVAR, and 75 km in FGAT. Even though the model resolution of 45 km is too coarse to resolve this supertyphoon, 4DVAR produces the strongest initial vortex among all the experiments with a minimum sea level pressure of 970 hPa. Thus, 4DVAR leads to the best intensity forecast.

The track forecast errors in kilometers and intensity forecast errors in hectopascals averaged over the 48-h forecast range are plotted in Fig. 6. It is evident that 4D-Var produces superior forecasts of both track and intensity for Typhoon Haitang over the 2-day period. Our analysis suggests that the initial vortex in the 4DVAR experiments is stronger than other schemes.

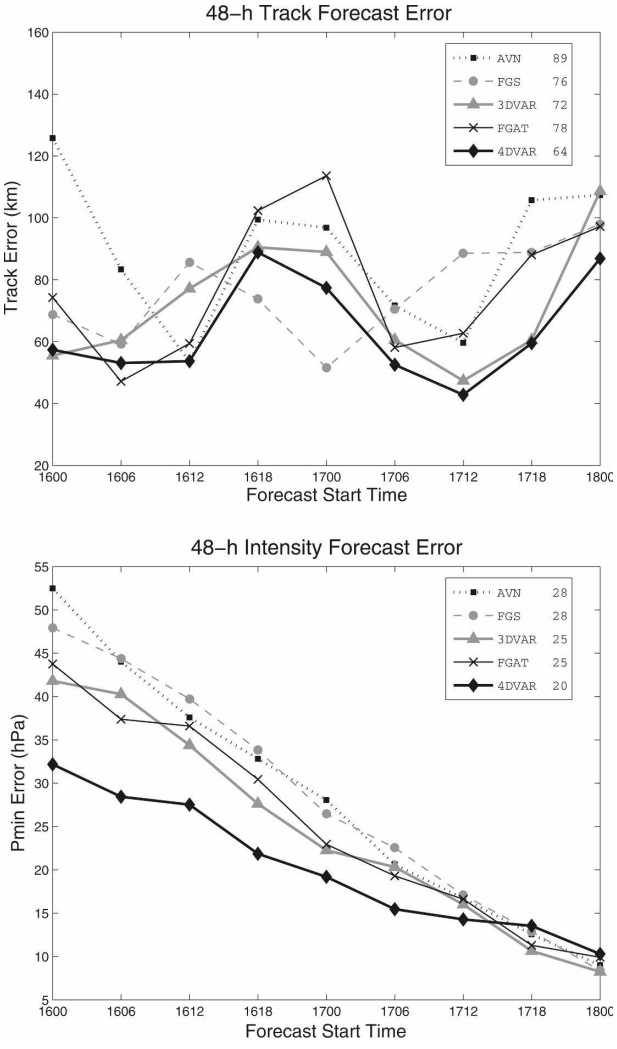

FIG. 6. The 48-h averaged forecast errors of (a) track (km) and (b) intensity (minimum sea level pressure, hPa) from FGS, AVN, 3DVAR, FGAT, and 4DVAR. The x axes are the forecast start times (day and hour). The numbers in the legends give the mean errors of all forecasts at different forecast times.

Its structure is more dynamically balanced, which leads to smaller initial adjustments. The absolute 6-h change in the minimum sea level pressure (maximum surface wind) averaged over all forecasts is 5.3 hPa (2.2 m s^{-1}) in 4DVAR in contrast to 11.1 hPa (5.5 m s^{-1}) in 3DVAR. The remedied vortex spinup contributes to better track and intensity forecasts. Further experiments will be carried out to assess the impact of different observation types, particularly the vortex bogus observations (Guo et al. 2006).

b. WRF 4D-Var experiments with cycling

To demonstrate that 4DVAR can be potentially useful for broader weather scenarios, a different case of heavy precipitation event that happened in Korea in a 4.5-day period from 1200 UTC 4 May to 0000 UTC 9 May 2006 was chosen. The impact of data assimilation using 3D-Var and 4D-Var in cycling mode on the precipitation forecast is assessed. During this 4.5-day time period, a cyclone moved eastward across the Korean peninsula and brought heavy rainfall to Korea.

TABLE 2. Number of observations assimilated by 3DVAR at 1200 UTC 4 May 2006.

	u	v	T	p	q
TEMP	459	464	519	—	385
SYNOP	67	59	73	71	72
PILOT	182	195	—	—	—
METAR	559	551	614	33	36
SHIP	1	1	2	2	1

In the designed experiments, the model domain covers the same area as the 10-km resolution domain 2 of the current Korea Meteorological Administration (KMA) regional numerical prediction system. To reduce the computation cost in our cycling experiments, we reduce the horizontal resolution to 30 km with 60 × 54 × 31 grid points. The assimilation is performed every 6 h followed by a 24-h forecast over this 4.5-day period. In cycling mode, the analysis uses the 6-h forecast from the previous analysis as the background.

The observations used in our data assimilation experiments include conventional observations and additional automatic weather station (AWS) data in South Korea [shown as the aviation routine weather report (METAR) in Tables 2 and 3]. As an example, we show in Table 2 and 3 the numbers of different observations at 1200 UTC 4 May 2006. The forecast model WRF ARW has the same physics options as chosen in the previous cold-start experiments. To evaluate the performance of WRF 4D-Var, two sets of experiments are carried out over the 4.5-day period:

- 3DVAR: 3D-Var is used to assimilate observations collected from −3 to +3 h around the analysis time. The procedure is similar to that described in the cold-start experiments. But it uses the 6-h forecast from

TABLE 3. Number of observations assimilated by 4DVAR at 1200 UTC 4 May 2006.

	u	v	T	p	q
TEMP	456	461	519	—	384
SYNOP	253	212	268	191	204
PILOT	185	194	—	—	—
METAR	2636	2402	2957	218	240
SHIP	1	1	2	2	1

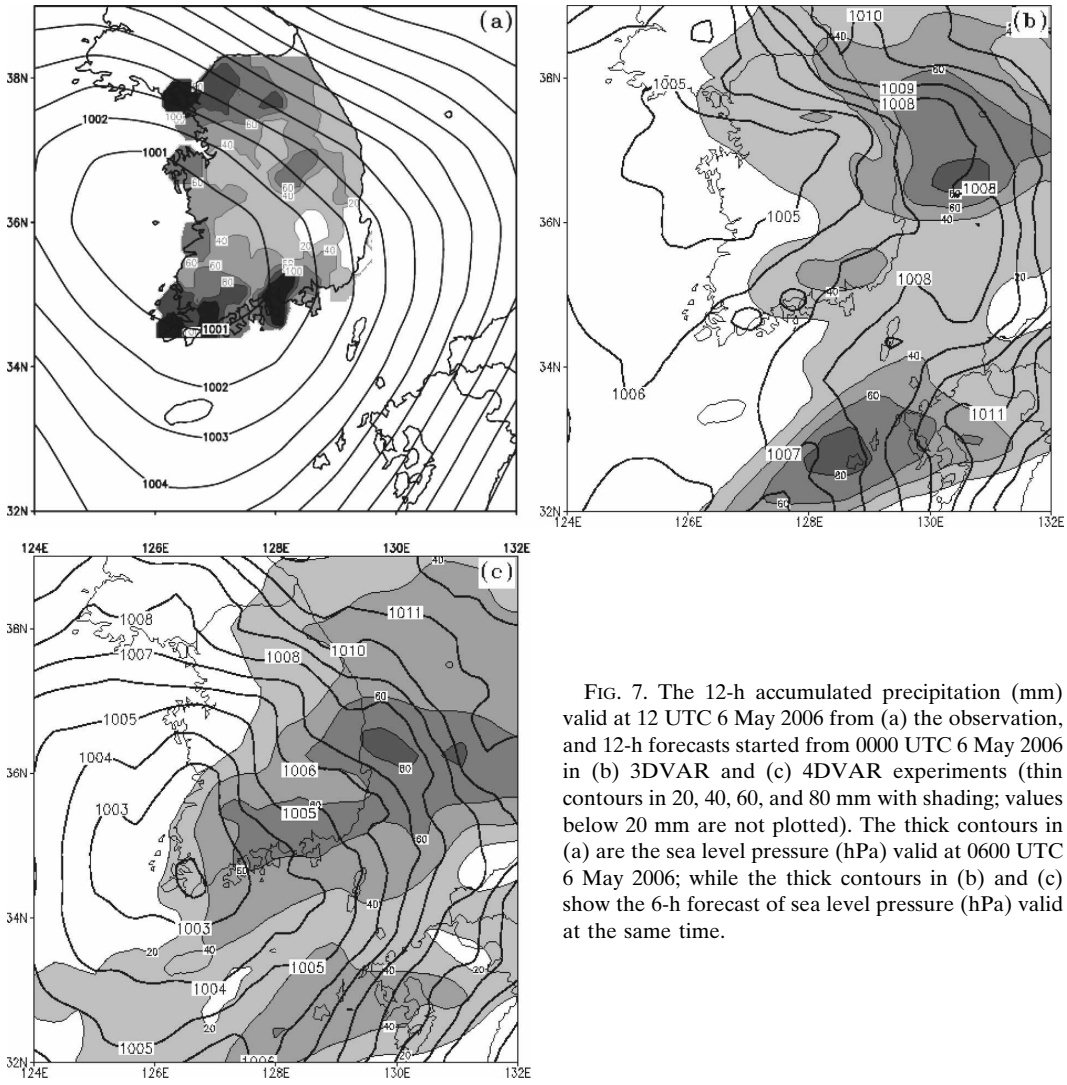

FIG. 7. The 12-h accumulated precipitation (mm) valid at 12 UTC 6 May 2006 from (a) the observation, and 12-h forecasts started from 0000 UTC 6 May 2006 in (b) 3DVAR and (c) 4DVAR experiments (thin contours in 20, 40, 60, and 80 mm with shading; values below 20 mm are not plotted). The thick contours in (a) are the sea level pressure (hPa) valid at 0600 UTC 6 May 2006; while the thick contours in (b) and (c) show the 6-h forecast of sea level pressure (hPa) valid at the same time.

the previous analysis as the background except in the very first cycle where the model states interpolated from the 30-km Korean operational model fields are used as the background. The lateral and lower boundary conditions are updated in the same way as previous 3DVAR experiment.

- 4DVAR: Similar to 3DVAR experiment except that 4D-Var is used for the analysis. The observations used in one 4DVAR analysis are listed in Table 3. Given an assimilation time window of 6 h, 4DVAR can assimilate high-frequency observations in an fixed observation network such as SYNOP or METAR, while 3DVAR can only assimilate one of such observations at a fixed location within the 6-h time window. The lateral and lower boundary conditions are updated in the same way as the 4DVAR experiment in previous case. The averaged computational cost for this case on *blueice* is about 3-h wall clock time for 50 iterations and 12 GB of memory on 64 processors. Within one iteration, the nonlinear, adjoint, and tangent linear models take 43, 130, and 45 s, respectively.

The performances of 4DVAR and 3DVAR are compared with special emphasis on the precipitation forecast. The heavy precipitation mainly occurred on 6 May when the cyclone was moving across Korea. Figure 7 shows the 12-h accumulated precipitation valid at 1200 UTC 6 May 2006 from the observation and 12-h forecasts started from 0000 UTC 6 May 2006 in 3DVAR and 4DVAR experiments. The heaviest rainfall (110–130 mm) occurred along the southern coast of Korea. The maximum rainfall over that area in the 3DVAR experiment is only about 40 mm, while 4DVAR pro-

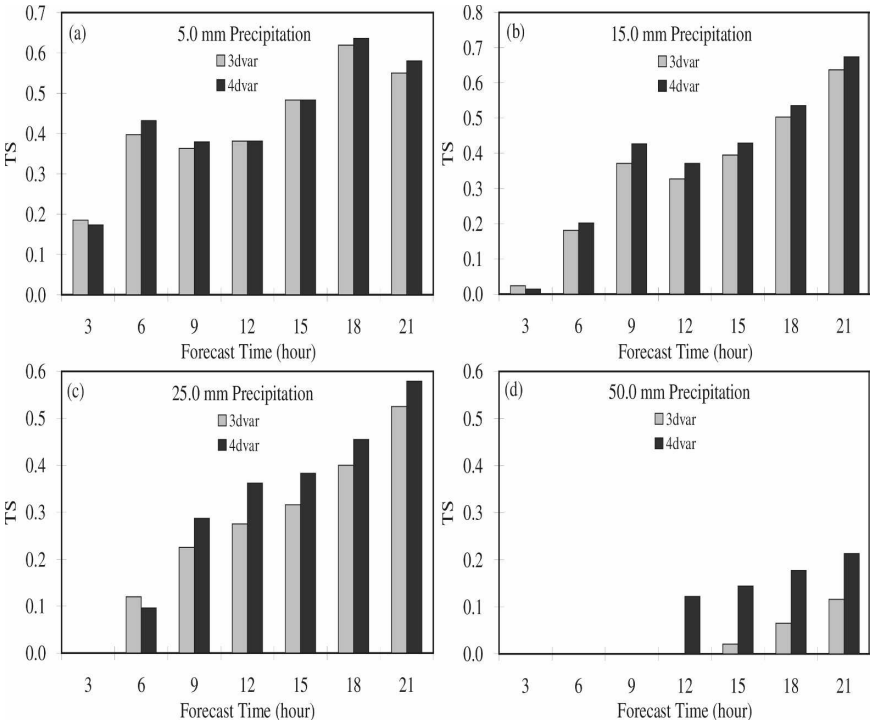

FIG. 8. Threats scores of precipitation amount of 5, 15, 25, and 50 mm.

duces 80-mm precipitation. Detailed analyses show that the differences in precipitation are primarily caused by the displacement of the cyclone as it crosses the peninsula. Comparing 3DVAR to 4DVAR experiment, as shown in Figs. 7b,c, the cyclone in 3DVAR was weaker so that the southerly and southwesterly flow in the southern part of the cyclone is weaker. Comparing to the sea level pressure in GFS analysis shown in Fig. 7a, 4DVAR produces a closer analysis than 3DVAR does. Less moisture is advected from the ocean toward the coast in the 3DVAR experiment than in the 4DVAR experiment. The moisture convergence and the upward vertical motions associated with the convection over the south coast region in 3DVAR are also significantly weaker than the 4DVAR experiments.

The overall precipitation forecast improvement can be indicated by comparing the precipitation threat scores. The threat score are computed at each forecast time at the 73 rain gauge locations in South Korea and then averaged over the 4.5-day period. The threat score (TS) is defined as

$$\mathrm{TS} = H/(H + M + F)$$

where H indicates a hit, event forecasted to occur and did occur; M indicates a miss, event forecasted not to occur but did occur; and F indicates a false alarm, event forecasted to occur but did not occur.

The threat scores of 5-, 15-, 25-, and 50-mm precipitation amounts are shown in Fig. 8. In general, the precipitation forecasts in the 4DVAR experiment over the 4.5-day period are significantly better than the 3DVAR experiment, especially for heavy rainfall forecast. For example, the threat score of threshold of 25 mm for the 18-h forecast increases from 0.4 to 0.45 and it jumps from 0.05 to 0.17 for a threshold of 50 mm.

5. Conclusions

This paper is a brief overview of the 4D-Var capability built on the multi-incremental formulation of WRF-Var. The current status of the WRF 4D-Var is a basic system with multiple executables, single or multiple processor capability, and the use of disk I/O to handle communication among the executables.

The structure functions of the 4D-Var are studied using single observation experiments. The example showed in this paper clearly demonstrates the flow-dependent nature of the analysis increments in a 6-h assimilation window: a small increment upstream of the observation at the beginning of the assimilation window, the intensification of the increment in time, and the final increment centered around the observation location with the structure stretched along the mean flow. The structure function and the increments in

single observations experiments helped us check the code and validate the linearization assumption made in the tangent linear and adjoint models.

Real-data experiments in both cold-start and cycling modes have been conducted. Within the WRF-Var framework, 4D-Var can assimilate most observation types available to 3D-Var (radiances have yet to be tested in 4D-Var). The 4D-Var algorithm can also assimilate more observations than 3D-Var from high-frequency fixed observing platforms, such as automated weather stations (AWS) networks. The results presented here indicate that 4D-Var is working properly and, on average, outperforms 3D-Var with similar configurations. Experiments with Typhoon Haitang (2005) using a cold-start setting during a 2-day period from 0000 UTC 16 to 0000 UTC 18 July 2005 clearly show that 4D-Var produces better track and intensity forecasts than 3D-Var and other schemes. Studies of a heavy rainfall case in Korea demonstrate that 4D-Var running in cycling mode can improve overall precipitation forecasts, especially the heavy rainfall forecasts, compared to 3D-Var runs. These encouraging results create bright prospects for operational applications.

Our experiments suggest that 4D-Var can assimilate more observations, and obtain dynamically balanced analysis with flow-dependent structures that then lead to better subsequent forecasts than its 3D-Var counterpart. There are also many tunable parameters in WRF-Var; for example, the variances and scale lengths of the background errors. Most of these parameters have been tuned for optimizing the performance of 3D-Var. In all the 4D-Var experiments conducted so far, none of these parameters have been modified. It should be expected that tuning of WRF-Var's observation/background error covariances should lead to further improvements in 4D-Var accuracy and efficiency. While we cannot draw conclusions from the limited case studies that WRF 4D-Var is superior to 3D-Var, the identified improvements are still encouraging. The performance of WRF 4D-Var demands evaluations over extended time periods. Nevertheless, the current results demonstrate the readiness of the community WRF 4D-Var system for data assimilation research.

The current WRF 4D-Var has a simple vertical diffusion scheme and a large-scale condensation scheme, in addition to the full WRF-ARW dynamics, in the tangent linear and adjoint models. Inclusion of additional physics in the tangent linear and adjoint models of WRF 4D-Var is planned in order to accommodate the needs of mesoscale analysis; for example, a linear microphysical parameterization model for the convective-scale assimilation of radar reflectivity observations. Since high-impact weather prediction is receiving more attention in recent years, further studies will be conducted to assess the impact of 4D-Var on WRF forecasts of severe weathers, such as heavy rainfall events, tropical cyclones, etc. Thorough evaluation of WRF 4D-Var will be reported in future papers.

Acknowledgments. The development of WRF 4D-Var has been primarily supported by the Air Force Weather Agency and the Korea Meteorological Administration. The authors would also like to thank Chris Snyder for his comments on an earlier version of the manuscript. Zhiquan Liu, Syed Rizvi, and Hongli Wang made significant contributions to this work. Thanks also to Fuqing Zhang and three anonymous reviewers for their constructive comments that helped improve this paper.

APPENDIX

WRF 4D-Var System Structure

Figure A1 depicts the data flow and program structure of WRF 4D-Var. Given the background model state $\mathbf{x}^b$, the lateral boundary conditions WRFBDY valid during the analysis time window, the background error covariance matrix $\mathbf{B}$, the observation error matrix $\mathbf{R}$, and the observations grouped into K time windows $(\mathbf{y}_1, \mathbf{y}_2, \ldots, \mathbf{y}_K)$, WRF 4D-Var will produce the analysis $\mathbf{x}^n$.

WRF, WRF$^+$, VAR, and COM are the four major components of WRF 4D-Var in terms of software structure. Each component is now described.

a. WRF

The ARW model (Skamarock et al. 2005) is referred to as WRF_NL. The ARW solves the compressible, nonhydrostatic Euler equations, cast in flux form and conserving of both mass and scalar. The ARW model has a terrain-following vertical coordinate and an Arakawa C-grid staggering in the horizontal. In addition to the wide range of physics options, the high-order numeric schemes include a third-order Runge–Kutta time-split integration scheme and a second- to sixth-order advection options. These advanced features make the ARW suitable for multiscale numerical simulations and forecasts.

b. WRF$^+$

WRF$^+$ comprises two models in one framework, namely the WRF tangent linear model (WRF_TL) and its adjoint (WRF_AD), which are compiled together into a single executable. The transformation of algorithms (TAF) in FORTRAN (Giering and Kaminski

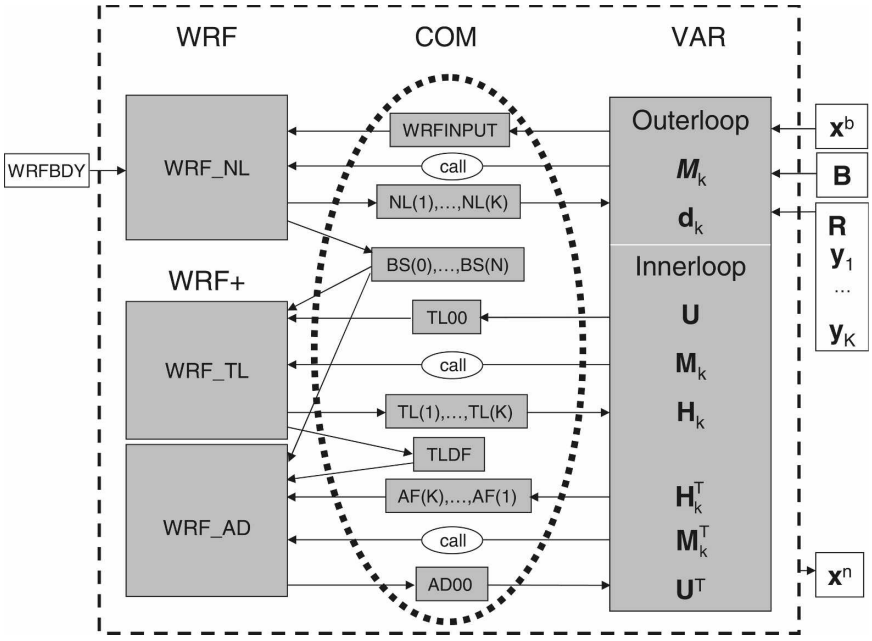

FIG. A1. The data flow and program structure of WRF 4DVAR. See text for definitions of symbols.

2003) was used to construct the tangent linear model and its adjoint from a simplified version of the full nonlinear WRF model (WRF_NL), which includes the full WRF-ARW dynamics, a large-scale condensation scheme, and a simple PBL scheme (formulated as vertical diffusion plus surface friction). Following Thépaut and Courtier (1991) and Navon et al. (1992), the tangent linear and adjoint codes were verified using the standard gradient tests and TL/AD tests procedure. The test results as well as some sensitivities studies using WRF_AD are reported in Xiao et al. (2008).

c. VAR

VAR contains all the components of WRF 3D-Var (Barker et al. 2005) extended to include four-dimensional enhancements such as the grouping of observations (i.e., splitting $\mathbf{y}$ into $\mathbf{y}_k$) and their related calculations (replacing H, $\mathbf{H}$, and $\mathbf{H}^{\mathrm{T}}$ by H_k, $\mathbf{H}_k$, and $\mathbf{H}_k^{\mathrm{T}}$) in an observation window (k), the function calls to WRF_NL, WRF_TL, and WRF_AD, and the grid/variable transform operators.

d. COM

Since WRF, WRF$^+$, and VAR are separate components, COM manages the communications among them. The implementation of COM is hidden from the other three components and allows the movement of data to be handled either through disk I/O, or through memory for maximum efficiency. When the I/O is done in memory instead of disk, an experiment with dimensions similar to those of our current case studies can be accelerated by up to 50%.

When the disk I/O is selected, the following files are used for the communication (in the order of appearance):

- WRFINPUT: The full model state at the beginning of each outerloop, written out by VAR and read in by WRF as initial model state.
- NL(1), . . . , NL(K): K model states, one for each observation window, produced by WRF and read in by VAR before computing the innovation vector $\mathbf{d}_k$.
- BS(0), . . . , BS(N): $N + 1$ model states, one for each time step, produced by WRF and read in by WRF$^+$ as basic states.
- TL00: The initial model state for the tangent linear model, written out by VAR after the $\mathbf{U}$ transform and read in by WRF$^+$.
- TL(1), . . . , TL(K): K (tangent linear) model states, one for each observation window, produced by WRF$^+$ during the tangent linear integration and read in by VAR before computing the adjoint forcing (AF) as defined below.
- TLDF: The digital filter forcing:

$$\sum_{i=0}^{N} f_i \mathbf{M}_i \mathbf{U} \mathbf{v}^n. \tag{A1}$$

As written out by WRF$^+$ at the end of the tangent linear integration and read in by WRF$^+$ at the beginning of the adjoint integration.

- AF(K), . . . , AF(1): K files containing adjoint forcings for each observation window k defined as

$$\mathbf{H}_k^{\mathrm{T}}\mathbf{R}^{-1}\{\mathbf{H}_k\mathbf{M}_k\mathbf{U}\mathbf{v}^n - \mathbf{d}_k\}. \quad \text{(A2)}$$

They are written by VAR and read in by WRF$^+$ during the adjoint integration.

- AD00: The output of WRF$^+$ after the adjoint model integration, read in by VAR before the $\mathbf{U}^{\mathrm{T}}$ transform.

Since the WRF 4D-Var prototype was built, it has been under continuous refinement in the recent two years (Huang et al. 2006). The basic system has the following features:

1) It runs as a combination of WRF (the released version 2.2), WRF$^+$ (the WRF tangent linear model and adjoint model), and WRF-Var (the release version 2.1 with 4D-Var extensions) executables.
2) It uses system calls to invoke three executables.
3) It uses disk I/O to handle the communications among WRF, WRF$^+$, and VAR.
4) It can run on a single processor as well as multiprocessors.
5) It has a penalty term, J_c, constructed using the digital filters to control noise during the minimization.
6) It includes a simple vertical diffusion with surface friction scheme to represent planetary boundary layer processes and a large-scale condensation scheme in the WRF tangent linear and adjoint models, as our initial addition to the full physics in WRF$^+$.

The parallel multiple program multiple data (MPMD) system architecture of WRF 4D-Var has demonstrated encouraging performance and made cycling data assimilation experiments possible. In WRF 4D-Var, the running time of one time step of adjoint model integration is typically 3 times longer than the nonlinear model integration. Future development will reduce the communication via disk I/O to improve the computational efficiency.

REFERENCES

Barker, D. M., W. Huang, Y.-R. Guo, A. J. Bourgeois, and Q. N. Xiao, 2004a: A three-dimensional variational data assimilation system for MM5: Implementation and initial results. *Mon. Wea. Rev.,* **132,** 897–914.

——, M. S. Lee, Y.-R. Guo, W. Huang, Q.-N. Xiao, and R. Rizvi, 2004b: WRF variational data assimilation development at NCAR. *Fifth WRF/14th MM5 Users' Workshop,* Boulder, CO, NCAR, 5 pp. [Available online at http://www.mmm.ucar.edu/mm5/workshop/ws04/Session5/dale.pdf.]

——, ——, ——, ——, S. Rizvi, and Q. Xiao, 2005: WRF-Var—A unified 3/4D-Var variational data assimilation system for WRF. *Sixth WRF/15th MM5 Users' Workshop,* Boulder, CO, NCAR, 17 pp. [Available online at http://www.mmm.ucar.edu/wrf/users/workshop/WS2005/presentations/session10/1-Barker.pdf.]

Buehner, M., 2005: Ensemble-derived stationary and flow-dependent background-error covariances: Evaluation in a quasi-operational NWP setting. *Quart. J. Roy. Meteor. Soc.,* **131,** 1013–1043.

Courtier, P., J.-N. Thépaut, and A. Hollingsworth, 1994: A strategy for operational implementation of 4D-Var, using an incremental approach. *Quart. J. Roy. Meteor. Soc.,* **120,** 1367–1387.

Gauthier, P., and J.-N. Thépaut, 2001: Impact of the digital filter as a weak constraint in the preoperational 4DVAR assimilation system of Météo France. *Mon. Wea. Rev.,* **129,** 2089–2102.

——, M. Tanguay, S. Laroche, and S. Pellerin, 2007: Extension of 3DVAR to 4DVAR: Implementation of 4DVAR at the Meteorological Service of Canada. *Mon. Wea. Rev.,* **135,** 2339–2364.

Giering, R., and T. Kaminski, 2003: Applying TAF to generate efficient derivative code of Fortran 77-95 programs. *PAMM,* **2,** 54–57.

Grell, G. A., and D. Devenyi, 2002: A generalized approach to parameterizing convection combining ensemble and data assimilation techniques. *Geophys. Res. Lett.,* **29,** 1693, doi:10.1029/2002GL015311.

Guo, Y. R., H.-C. Lin, X. X. Ma, X.-Y. Huang, C. T. Terng, and Y.-H. Kuo, 2006: Impact of WRF-Var (3DVar) background error statistics on typhoon analysis and forecast. *Seventh WRF Users' Workshop,* Boulder, CO, NCAR, 7 pp. [Available online at http://www.mmm.ucar.edu/wrf/users/workshops/WS2006/abstracts/PSession04/P4_2_Guo.pdf.]

Gustafsson, N., 1992: Use of a digital filter as weak constraint in variational data assimilation. *Proc. Workshop on Variational Assimilation, with Special Emphasis on Three-Dimensional Aspects,* Reading, United Kingdom, ECMWF, 327–338.

Honda, Y., M. Nishijima, K. Koizumi, Y. Ohta, K. Tamiya, T. Kawabata, and T. Tsuyuki, 2005: A pre-operational variational data assimilation system for a non-hydrostatic model at the Japan Meteorological Agency: Formulation and preliminary results. *Quart. J. Roy. Meteor. Soc.,* **131,** 3465–3475.

Hong, S.-Y., J. Dudhia, and S.-H. Chen, 2004: A revised approach to ice microphysical processes or the bulk parameterization of clouds and precipitation. *Mon. Wea. Rev.,* **132,** 103–120.

Huang, X.-Y., X. Yang, N. Gustafsson, K. Mogensen, and M. Lindskog, 2002: Four-dimensional variational data assimilation for a limited area model. HIRLAM Tech Rep 57, 41 pp. [Available from SMHI, S-601 76 Norrkoping, Sweden.]

——, Q. Xiao, W. Huang, D. Barker, Y.-H. Kuo, J. Michalakes, and Z. Ma, 2005: The weather research and forecasting model based on the 4-dimensional variational data assimilation system. [WRF-(4D)Var]. *Sixth WRF/15th MM5 Users' Workshop,* Boulder, CO, NCAR, 15 pp. [Available online at http://www.mmm.ucar.edu/wrf/users/workshops/WS2005/presentations/session10/5-Huang.pdf.]

——, and Coauthors, 2006: Preliminary results of WRF 4D-Var. *Seventh WRF Users' Workshop,* Boulder, CO, NCAR, 20 pp. [Available online at http://www.mmm.ucar.edu/wrf/users/workshops/WS2006/presentations/Session4/4_5.pdf.]

Jang, K.-I., X. Zou, M. Pondeca, M. Shapiro, C. Davis, and A.

Krueger, 2003: Incorporating TOMS ozone measurements into the prediction of the Washington, D.C., winter storm during 24–25 January 2000. *J. Appl. Meteor.,* **42,** 797–812.

Lee, M.-S., and D. Barker, 2005: Preliminary tests of first guess at appropriate time (FGAT) with WRF 3DVAR and WRF model. *J. Kor. Meteor. Soc.,* **41,** 495–505.

Le Dimet, F., and O. Talagrand, 1986: Variational algorithms for analysis and assimilation of meteorological observations: Theoretic aspects. *Tellus,* **38A,** 97–110.

Lewis, J., and J. Derber, 1985: The use of adjoint equations to solve a variational adjustment problem with advective constraints. *Tellus,* **37A,** 309–327.

Lorenc, A. C., 2003: Modelling of error covariances by 4D-Var data assimilation. *Quart. J. Roy. Meteor. Soc.,* **129,** 3167–3182.

——, and F. Rawlins, 2005: Why does 4D-Var beat 3D-Var? *Quart. J. Roy. Meteor. Soc.,* **131,** 3247–3257.

Lynch, P., and X.-Y. Huang, 1992: Initialization of the HIRLAM model using a digital filter. *Mon. Wea. Rev.,* **120,** 1019–1034.

Navon, I. M., X. Zou, J. Derber, and J. Sela, 1992: Variational data assimilation with an adiabatic version of the NMC spectral model. *Mon. Wea. Rev.,* **120,** 1433–1446.

Parrish, D. F., and J. C. Derber, 1992: The National Meteorological Center's spectral statistical-interpolation analysis system. *Mon. Wea. Rev.,* **120,** 1747–1763.

Rabier, F., and Coauthors, 1997: Recent experimentation on 4D-var and first results from a simplified Kalman filter. ECMWF Tech. Memo. 240, Reading, United Kingdom, 42 pp.

——, H. Järvinen, E. Klinker, J.-F. Mahfouf, and A. Simmons, 2000: The ECMWF operational implementation of four dimensional variational assimilation. *Quart. J. Roy. Meteor. Soc.,* **126,** 1143–1170.

Rawlins, F., S. P. Ballard, K. J. Bovis, A. M. Clayton, D. Li, G. W. Inverarity, A. C. Lorenc, and T. J. Payne, 2007: The Met Office global 4-Dimensional data assimilation system. *Quart. J. Roy. Meteor. Soc.,* **133,** 347–362.

Ruggiero, F. H., J. Michalakes, T. Nehrkorn, G. D. Modica, and X. Zou, 2006: Development of a new distributed-memory MM5 adjoint. *J. Atmos. Oceanic Technol.,* **23,** 424–436.

Skamarock, W. C., J. B. Klemp, J. Dudhia, D. O. Gill, D. M. Barker, W. Wang, and J. G. Powers, 2005: A description of the advanced research WRF version 2. NCAR Tech. Note TN-468+STR, 88 pp.

Sun, J., and N. A. Crook, 1997: Dynamical and microphysical retrieval from Doppler radar observations using a cloud model and its adjoint. Part I: Model development and simulated data experiments. *J. Atmos. Sci.,* **54,** 1642–1661.

Thépaut, J.-N., and P. Courtier, 1991: Four dimensional variational data assimilation using the adjoint of a multilevel primitive-equation model. *Quart. J. Roy. Meteor. Soc.,* **117,** 1225–1254.

——, ——, G. Belaud, and G. Lemaitre, 1996: Dynamic structure functions in a four-dimensional variational assimilation: A case study. *Quart. J. Roy. Meteor. Soc.,* **122,** 535–561.

Veersé, F., and J.-N. Thépaut, 1998: Multi-truncation incremental approach for four-dimensional variational data assimilation. *Quart. J. Roy. Meteor. Soc.,* **124,** 1889–1908.

Wee, T.-K., and Y.-H. Kuo, 2004: Impact of a digital filter as a weak constraint in MM5 4DVAR. *Mon. Wea. Rev.,* **132,** 543–559.

Xiao, Q., Y.-H. Kuo, Z. Ma, W. Huang, X.-Y. Huang, X.-Y. Zhang, D. M. Barker, J. Michalakes, and J. Dudhia, 2008: Application of an Adiabatic WRF adjoint to the investigation of the May 2004 McMurdo Antarctica severe wind event. *Mon. Wea. Rev.,* **136,** 3696–3713.

Xu, L., T. Rosmond, and R. Daley, 2005: Development of NAVDAS-AR: Formulation and initial tests of the linear problem. *Tellus,* **57A,** 546–559.

Zhang, F., 2005: Dynamics and structure of mesoscale error covariance of a winter cyclone estimated through short-range ensemble forecasts. *Mon. Wea. Rev.,* **133,** 2876–2893.

——, C. Snyder, and R. Rotunno, 2002: Mesoscale predictability of the "Surprise" snowstorm of 24–25 January 2000. *Mon. Wea. Rev.,* **130,** 1617–1632.

——, ——, and ——, 2003: Effects of moist convection on mesoscale predictability. *J. Atmos. Sci.,* **60,** 1173–1185.

——, N. Bai, R. Rotunno, C. Snyder, and C. C. Epifanio, 2007: Mesoscale predictability of moist baroclinic waves: Convection-permitting experiments and multistage error growth dynamics. *J. Atmos. Sci.,* **64,** 3579–3594.

Zou, X., Y.-H. Kuo, and Y.-R. Guo, 1995: Assimilation of atmospheric radio refractivity using a nonhydrostatic mesoscale model. *Mon. Wea. Rev.,* **123,** 2229–2249.

——, F. Vandenberghe, M. Pondeca, and Y.-H. Kuo, 1997: Introduction to adjoint techniques and he MM5 adjoint modeling system. NCAR Tech. Note NCAR/TN-435-STR, 110 pp.

Zupanski, D., D. F. Parrish, E. Rogers, and G. DiMego, 2002: Four-dimensional variational data assimilation for the blizzard of 2000. *Mon. Wea. Rev.,* **130,** 1967–1988.

Zupanski, M., 1993: Regional four-dimensional variational data assimilation in a quasi-operational forecasting environment. *Mon. Wea. Rev.,* **121,** 2396–2408.

——, D. Zupanski, T. Vukicevic, K. Eis, and T. V. Haar, 2005: CIRA/CSU four-dimensional variational data assimilation system. *Mon. Wea. Rev.,* **133,** 829–843.